ChemCatChem

Supporting Information

Rhodium Single-Atom Catalysts on Titania for Reverse Water Gas Shift Reaction Explored by First Principles Mechanistic Analysis and Compared to Nanoclusters

Francis Doherty and Bryan R. Goldsmith*

Table of Contents

S1. Genetic algorithm details for modeling nanoclusters on titania

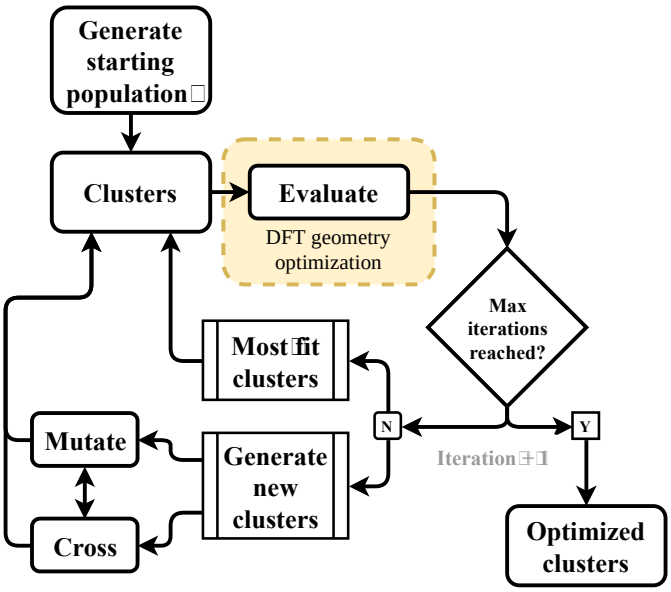

Fig. S1. Workflow summarizing the genetic algorithm for the global optimization of supported nanoclusters. Initially, a starting population of clusters is generated, which are then evaluated by DFT-based geometry optimization. The clusters are next evolved via mutate and crossover operations and the new clusters have their energies evaluated using DFT. This cycle is repeated until either the number of max iterations is reached, or no new low-energy structures are found.

The calculated total electronic energy was used to evaluate the fitness of each nanocluster's structure. The fitness function of i^{th} candidate (F_i) is:

$$F_i = ½[1 - \tanh(2\rho_i - 1)] \quad \text{(S1)}$$

$$\rho_i = (E_i - E_{min})/(E_{max} - E_{min}) \quad \text{(S2)}$$

where E_i is the energy of the i^{th} candidate, and E_{max} and E_{min} denote the maximum and minimum energy of any structure in the population. Each structure has a probability of being selected for a crossover operation based on its fitness value divided by the sum fitness of the total generation. Each generation had a total of 12 different structures to analyze. New structures are generated by the crossover operation and used to fill out a new generation. There is also a 30% probability of mutation occurring, where one cluster will be randomly rotated or one atom in the cluster will be translated in space, and then this cluster is added to the population for fitness evaluation. The process continues until no new lowest energy structures are found within 1000 structures tested via DFT or after 80 generations, whichever comes first.

S2. Rh_1/TiO_2 species and rWGSR reaction pathway modeling

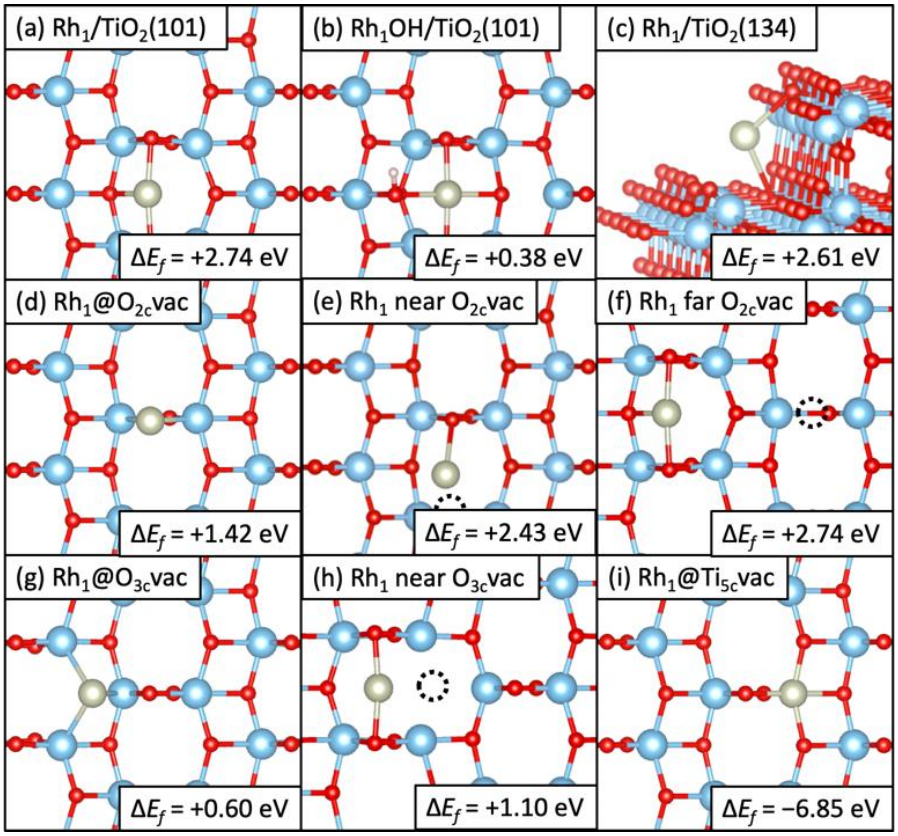

Fig. S2. Top view of the Rh_1 binding locations on anatase TiO_2 surfaces, along with the formation energy of supported Rh_1 (ΔE_f) relative to a TiO_2 surface (clean, defective, or step, as relevant) and bulk Rh. The systems considered were: (a) Rh_1 on TiO_2(101), (b) Rh_1 on TiO_2(101) with a nearby hydroxyl group, (c) Rh_1 on the TiO_2(134) step edge, (d) Rh_1 occupying an O vacancy at the two-fold coordinated site (@O_{2c}vac) on TiO_2(101), (e) Rh_1 with an O_{2c}vac nearby on TiO_2(101), (f) Rh_1 with an O_{2c}vac far away on TiO_2(101), (g) Rh_1 occupying an O vacancy at the three-fold coordinated site (@O_{3c}vac) on TiO_2(101), (h) Rh_1 near a O_{3c}vac on TiO_2(101) and (i) Rh_1 in a Ti vacancy at the five-fold coordinated site (@Ti_{5c}vac) on TiO_2(101). Oxygen vacancies are denoted with dashed circles. Atom color legend: Blue = Ti, Red = O, Gray = Rh.

Microkinetic modeling details. The elementary steps used in each constructed microkinetic model are shown in **Table S1**. The * denotes a Rh_1 site, $O_{lattice}$ denote lattices oxygen in the TiO_2 support, and O_{vac} denotes an oxygen vacancy in the TiO_2 support.

Table S1. Elementary reaction steps for microkinetic models of $Rh_1/TiO_2(101)$, Rh_1OH/TiO_2 and Rh_1 near O_{3c}vac at 400 K. Forward and reverse barriers given as input into the microkinetic simulations at 400 K. The corresponding degree of rate control output is also given. Empty cells (--) for forward or reverse barrier refer to reactions that are considered to have no barrier in that direction.

Elementary reaction steps for $Rh_1/TiO_2(101)$ via carboxyl (COOH) mechanism

Elementary Step	Forward barrier	Reverse barrier	Corresponds to Fig. 3a in main text	Degree of Rate Control
$H_{2(g)} + * \rightleftharpoons H_2*$	--	0.73 eV	i. → ii.	0.00
$CO_{2(g)} + * \rightleftharpoons CO_2*$	--	0.83 eV	i. → ii. (alt)[a]	0.00
$CO_{2(g)} + H_2* \rightleftharpoons CO_2,H_2*$	--	0.57 eV	ii. → iii.	0.00
$CO_2* + H_{2(g)} \rightleftharpoons CO_2,H_2*$	--	0.47 eV	ii. → iii. (alt)	0.00
$CO_2,H_2* \rightleftharpoons COOH,H*$	0.34 eV	1.05 eV	iii. → TS1 → iv.	0.00
$COOH,H* \rightleftharpoons CO* + H_2O_{(g)}$	1.93 eV	1.12 eV	iv. → TS2 → v.	1.00
$CO* \rightleftharpoons CO_{(g)} + *$	1.87 eV	--	v. → i.	0.00

[a] alt refers to the alternative order of adsorption for CO_2 and H_2. Both are provided in the model to allow for flexibility in the adsorption order.

Elementary reaction steps for $Rh_1OH/TiO_2(101)$ via carboxyl (COOH) mechanism

Elementary Step	Forward barrier	Reverse barrier	Corresponds to Fig. 3b in main text	Degree of Rate Control
$H_{2(g)} + * \rightleftharpoons H_2*$	--	0.72 eV	i. → ii.	0.00
$H_2* + O_{lattice} \rightleftharpoons H* + HO_{lattice}$	0.38 eV	1.00 eV	ii. → TS1 → iii.	0.00
$CO_{2(g)} + H* + HO_{lattice} \rightleftharpoons CO_2,H* + HO_{lattice}$	--	0.11 eV	iii. → iv.	0.00
$CO_2,H* + HO_{lattice} \rightleftharpoons COOH* + HO_{lattice}$	0.36 eV	1.15 eV	iv. → TS2 → v.	0.00
$COOH* + HO_{lattice} \rightleftharpoons COOH,H* + O_{lattice}$	1.39 eV	0.30 eV	v. → TS3 → vi.	0.00
$COOH,H* \rightleftharpoons CO* + H_2O_{(g)}$	1.42 eV	1.68 eV	vi. → TS4 → vii.	1.00
$CO* \rightleftharpoons CO_{(g)} + *$	2.05 eV	--	vii. → i.	0.00

Elementary reaction steps for Rh_1 near O_{3c}vac via CO_2 dissociation mechanism

Elementary Step	Forward barrier	Reverse barrier	Corresponds to Fig. 4 in main text	Degree of Rate Control
$H_{2(g)} + * \rightleftharpoons H_2*$	--	0.73 eV	i. → ii.	0.00
$H_2* + O_{lattice} \rightleftharpoons H* + HO_{lattice}$	0.62 eV	0.09 eV	ii. → TS1 → iii.	0.00
$H* + HO_{lattice} \rightleftharpoons H_2O_{(g)} + * + O_{3c}vac$	0.98 eV	--	iii. → iv.	1.00
$CO_{2(g)} + * \rightleftharpoons CO_2*$	0.21 eV	--	iv. → TS2	0.00
$CO_2* + O_{3c}vac \rightleftharpoons CO* + O_{lattice}$	--	2.20 eV	TS2 → v.	0.00
$CO* \rightleftharpoons CO_{(g)} + *$	1.87 eV	--	v. → i.	0.00

Forward and backward reaction rate constants were computed using the DFT-calculated activation barriers. For surface reactions, forward and backward rate constants for each step were determined by the Arrhenius equation:

$$k_i = Ae^{\frac{\Delta G_i^{\ddagger}}{k_b T}} \tag{S5}$$

where k_i is the reaction rate constant of step i in s^{-1}. Here k_b, T, and $\Delta G^{\ddagger}$ are the Boltzmann constant, temperature, and the activation free energy barrier, respectively. The pre-factor A is approximated as 10^{13} s^{-1} for all surface reactions. $\Delta G^{\ddagger}$ for surface reactions include the hindered rotational and vibrational entropy and enthalpy of each bound intermediate calculated at 400 K.

The rate of molecular adsorption is determined by the Hertz-Knudsen equation:

$$k_{ads} = \frac{pA'}{\sqrt{2\pi m k_b T}} S \tag{S6}$$

where p is the partial pressure of adsorbate in the gas phase, A' is the surface area of the adsorption site, m is the mass of the adsorbate molecule and S is the sticking coefficient. A' is approximated as 1.0 $Å^2$ (10^{-20} m^2), and S is assumed to be 1.0.

The rate of desorption considers the added entropy from the adsorbate returning to the gas phase. There are assumed to be three rotational degrees of freedom and two translational degrees of freedom in the transition state. Thus, the rate of desorption is given by:

$$k_{des} = \frac{k_b T^3}{h^3} \frac{A'(2\pi k_b)}{\sigma \theta_{rot}} e^{-\frac{E_{des}}{k_b T}} \tag{S7}$$

where σ is the symmetry number, θ is the characteristic temperature for rotation, and E_{des} is the electronic desorption energy from DFT (without zero-point correction).

Differential equations for all the surface reaction intermediates were constructed using the rate constants and the set of elementary reaction steps. The elementary and overall reaction rates, degrees of rate control, and apparent activation barriers were calculated by the MKMCXX program.

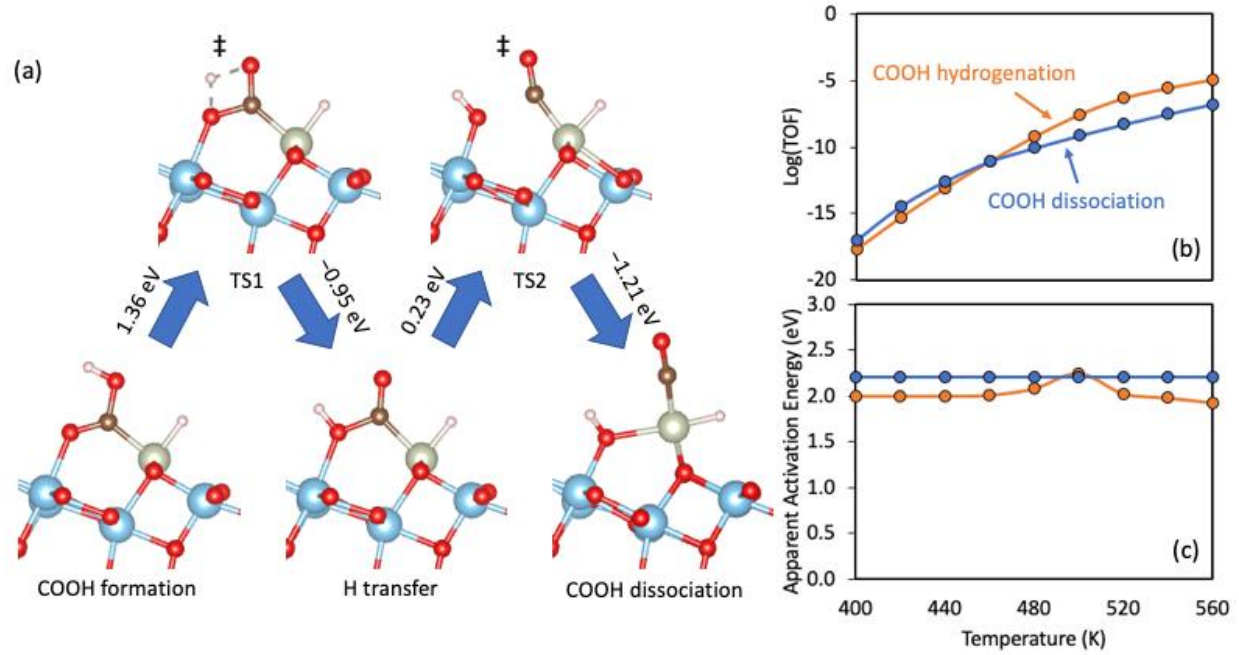

Fig. S3. Alternative mechanism steps for *COOH dissociation to *CO and *OH on $Rh_1/TiO_2(101)$. (a) Geometries of stable intermediates and transition states along the alternate pathway, highlighting steps that differ significantly from original mechanism (**Fig. 3a**). Energy differences between geometries are given. (b) TOF vs. temperature and (c) apparent activation energy vs. temperature for the overall reaction mechanism, comparing the alternative *COOH dissociation pathway (blue) to the original *COOH hydrogenation pathway (orange).

S3. Rh nanocluster geometry and properties

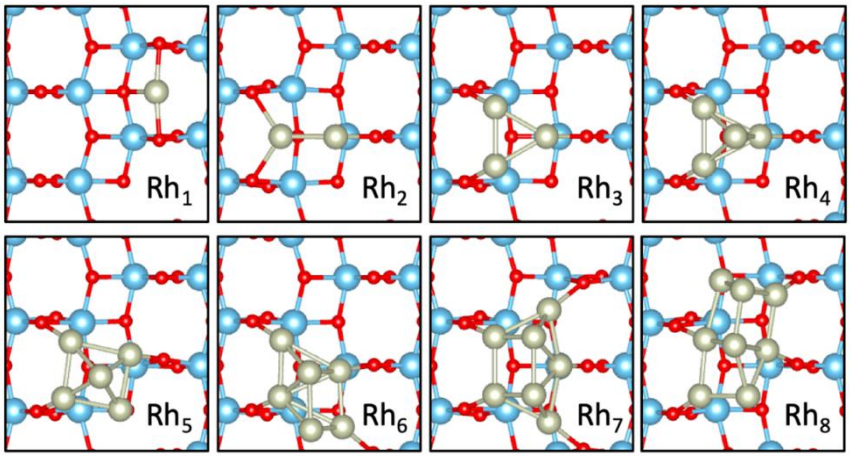

Fig. S4. Most stable configurations of Rh_x/TiO_2 (x = 1–8 atoms). Nanocluster sizes of four atoms and larger were generated by the genetic algorithm, whereas Rh_1, Rh_2, and Rh_3 were found by manually searching different structures and locations on the support. Atom color legend: Blue = Ti, Red = O, Gray = Rh.

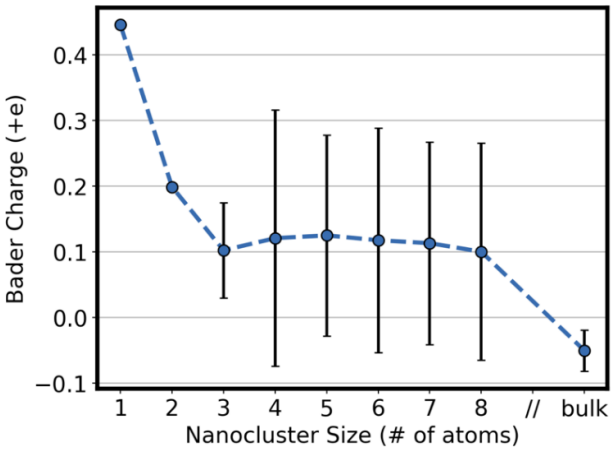

Fig. S5. Rh nanocluster characterization by Bader charge analysis. Bader charge is given as an average of all atoms in each cluster (blue dots). Black bars denote the range of atomic charge within each nanocluster. This data corresponds to the bare nanoclusters shown in **Fig**. **S3**. Dashed blue line is to guide the eyes.

Sampling CO, CO_2, and H_2 adsorption configurations on Rh clusters. Low energy adsorption configurations were found by sampling 19 different adsorption configurations radially distributed around each cluster. For each cluster, the center of mass and maximum cluster radius was calculated. The adsorbate starting positions were determined by distributing evenly around the cluster in polar coordinates. Adsorbate radius was set to the cluster radius plus 2 Å, azimuthal angle phi ranged from 0° to 300° in increments of 60°, and the polar angle theta ranged from 0° to 90° in increments of 30°. CO molecules were rotated to point perpendicularly away from the cluster surface. CO_2 and H_2 adsorption configurations were sampled similarly and were rotated to be parallel to the cluster surface. Adsorbates were relaxed via geometry optimization, and the final configuration with the strongest binding energy was reported.

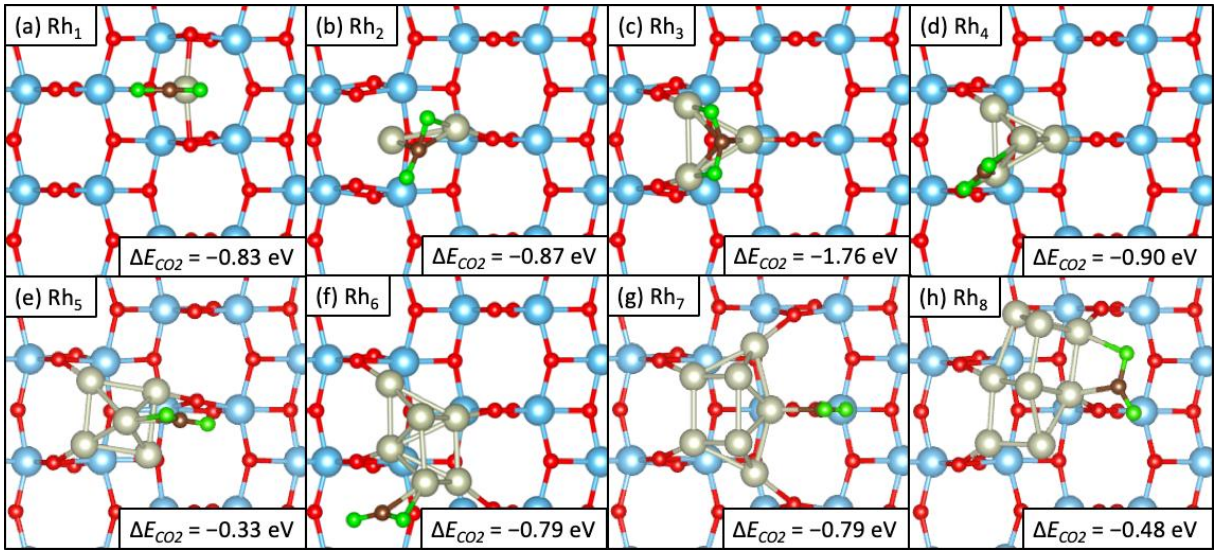

Fig. S6. Geometries of CO_2 on Rh_x/TiO_2 (x = 1–8 atoms), with corresponding electronic adsorption energies of CO_2 (ΔE_{CO2}) shown inset. Atom color legend: Blue = Ti, Red = O, Gray = Rh, Green = O in CO_2, Brown = C.

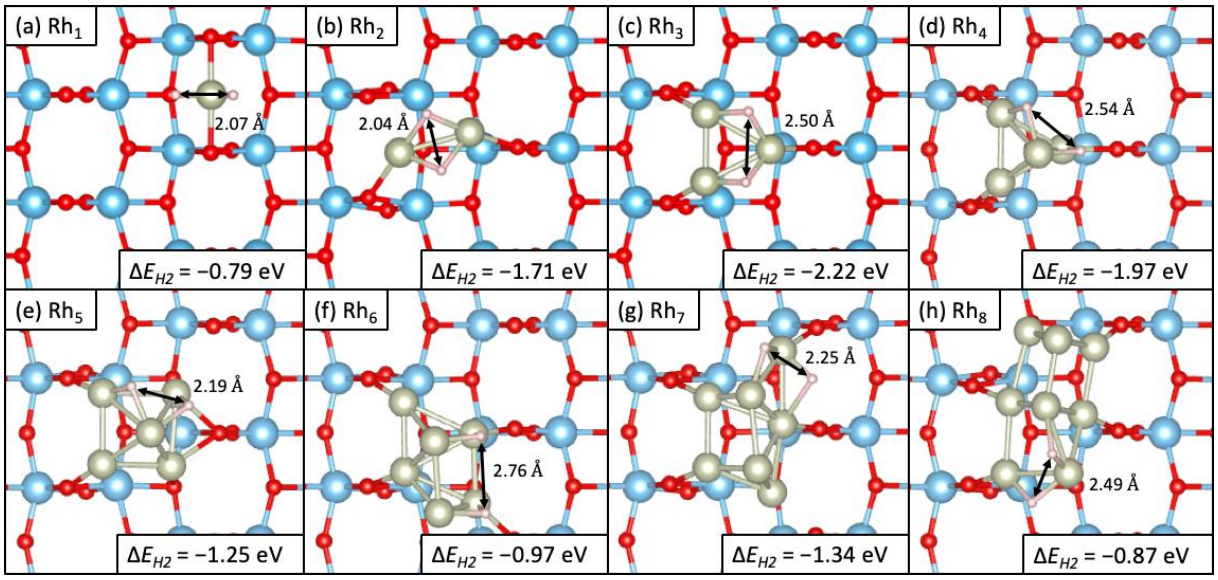

Fig. S7. Geometries of dissociated H_2 on Rh_x/TiO_2 (x = 1–8 atoms), with corresponding electronic adsorption energies (ΔE_{H2}) shown inset and H-H distances given. Atom color legend: Blue = Ti, Red = O, Gray = Rh, White = H.

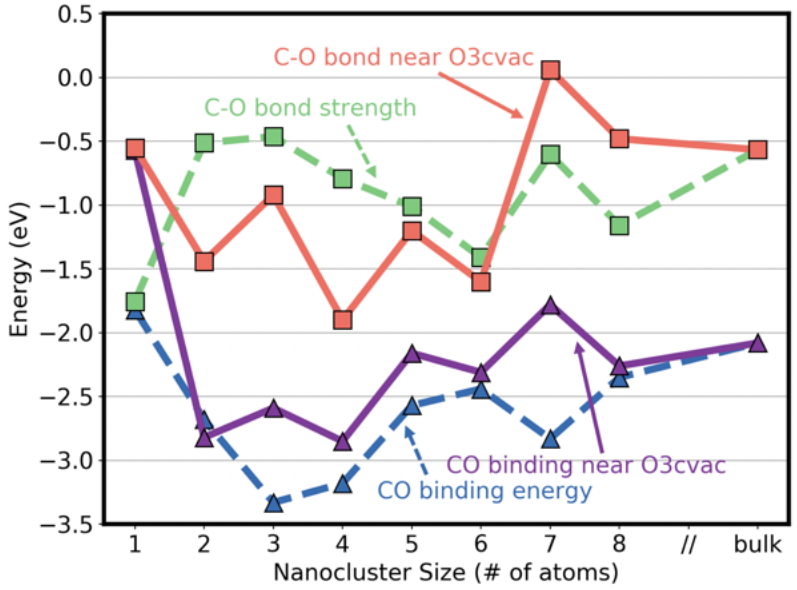

Fig. S8. CO binding energy (blue, purple) and C-O bond strength (green, orange) on Rh_x/TiO_2 (x = 1–8 atoms) and bulk Rh(111). Dashed lines indicate undefected supports (data appearing in Fig. 7 of main text), and solid lines indicate the inclusion of a nearby O_{3c}vac in TiO_2. O vacancy causes changes to C-O bond strength, but Rh_1 still has uniquely weak CO binding energy comparable to the C-O bond strength.